Available online at www.sciencedirect.com

SciVerse ScienceDirect

Ceramics International 38 (2012) 4097–4103

CERAMICS INTERNATIONAL

www.elsevier.com/locate/ceramint

Mössbauer, magnetic and microwave absorption characteristics of substituted W-type hexaferrites nanoparticles

Muhammad Javed Iqbal [a,*], Rafaqat Ali Khan [a], Shigemi Mizukami [b], Terunobu Miyazaki [b]

[a] Surface and Solid State Chemistry Laboratory, Department of Chemistry, Quaid-I-Azam University, Islamabad 45320, Pakistan
[b] WPI Advanced Institute for Material Research, Tohoku University, 2-1-1 Katahira, 980-8577 Sendai, Japan

Received 29 November 2011; received in revised form 16 January 2012; accepted 25 January 2012
Available online 1 February 2012

Abstract

W-type hexaferrite nanoparticles of nominal composition $BaCo_{2-x}Mn_xFe_{16-2y}Zr_yNi_yO_{27}$ ($x = 0–0.5$; $y = 0–1.0$), are synthesized by using the chemical co-precipitation technique. The X-ray diffraction (XRD) data conform to the formation of single phase. Mössbauer analysis reveals that extrinsic substitution of metal ions (Mn_x and Zr_y–Ni_y) takes place at 2d, f_{IV}, 2b, and 12k sub-lattices. Doped metal substitution up to ionic contents of $x = 0.3$ and $y = 0.6$, results in enhancement of the saturation magnetization M_s and remanent magnetization M_r while these substitutions lower the coercivity H_c. The optimum values of the above mentioned three parameters, measured at room temperature, using a vibrating sample magnetometer (VSM), are 79.7 emu g^{-1}, 36.0 emu g^{-1} and 1012 Oe, respectively. Microwave absorption characteristics calculated from complex permeability and complex permittivity data retrieved by a vector network analyzer (VNA) increase as the doped metal ions content increases.

Keywords: A. Powders: chemical preparation; C. Magnetic properties; D. Ferrites; Mössbauer spectroscopy; Microwave absorption

1. Introduction

With the advent of modern electrical, microwave and magnetic devices, the electromagnetic interference has become a serious problem. It is therefore important to design material that can attenuate electromagnetic radiations. W-type hexaferrites offer superior magnetic and microwave absorption characteristics as compared to the other coordination hexagonal ferrites and has potential for applications in magnetic and microwave devices. Owing to dielectric and magnetic behavior, W-type hexaferrites are considered indispensable for electromagnetic interference attenuation and microwave absorption purposes. The cell structure of W-hexaferrites as reported in the literature [1–3] suggests that cations in W-hexaferrites, except Ba^{2+}, occupy seven non-equivalent sub-lattices within the R- and S-blocks, i.e. 12k, $4f_{VI}$, 6g, 4f (octahedral coordination), 4e, $4f_{IV}$ (tetrahedral coordination) and 2d (bipyramidal coordination). The prefix denotes the number of cations present in the particular sub-lattice in a single unit cell. Different metallic ions in the R- and S-blocks have spin aligned along the easy *c*-axis, for instance the cations that occupy 12k, 6g, 4f and 2d sites have electronic spin in upward direction but those occupying 4e, $4f_{IV}$ and $4f_{VI}$ sub-lattice sites have electronic spin in downward direction [1]. This diversity provides a convenient possibility by extrinsically substituting divalent and trivalent metallic ions to alter at will the electrical and magnetic properties.

Substitution of La^{3+} for large divalent Ba^{2+} ions, i.e. in $BaZn_{0.5}Mg_{0.5}Fe_{16}O_{27}$, enhanced the electrical resistivity and dielectric constant of the product. The Curie temperature has been previously reported to decrease with the increment of the dopant contents [4]. Doping with Nd^{3+} ions varied the microstructure and improved the microwave absorption characteristics of $BaCo_2Fe_{16}O_{27}$ hexaferrites [5]. Different oxides such as antimony doped tin oxide (ATO) and vanadium pentoxide (V_2O_5) considerably improved electromagnetic properties of ferrites [6,7]. Doping of $BaZn_2Fe_{16}O_{27}$ with Co^{2+} on divalent ionic site of Zn^{2+} is known to reduce the saturation magnetization [8] and Mg^{2+} ions incorporated at divalent ionic sites in $BaCoZnFe_{16}O_{27}$ showed an increased magnetic susceptibility [9].

* Corresponding author. Tel.: +92 51 90642143; fax: +92 51 90642241.
E-mail address: mjiqauchem@yahoo.com (M.J. Iqbal).

0272-8842/$36.00
doi:10.1016/j.ceramint.2012.01.067

Synthesis of nanometric size particles of W-type hexaferrites by cost effective and simple chemical route is of utmost importance. For this purpose, a number of synthesis methods are in practice including sol–gel, micro-emulsion [10,11], machano-activation [12], two-step synthesis [13], and chemical co-precipitation [14,15]. We have synthesized nanoparticles of Ba-W type hexaferrites by the chemical co-precipitation method. This method is cost effective and more likely to produce a single-phase material, i.e. $BaCo_2Fe_{16}O_{27}$. In the present work, we have attempted to dope a rare combination of Mn^{2+}, Zr^{4+} and Ni^{2+} in the formulation of Ba-W type hexaferrites. The Mn^{2+} ion is substituted on Co^{2+} ionic site and a binary mixture of Zr^{4+} + Ni^{2+} is doped to partially replace Fe^{3+} ions. The reason for selection of the above-mentioned ions is their prominent effects on the crystalline anisotropy, which in turn would affect the magnetic properties at high frequencies.

2. Experimental

W-type hexaferrites of nominal composition $BaCo_{2-x}Mn_xFe_{16-2y}Zr_yNi_yO_{27}$ (where $x = 0$, 0.1, 0.2, 0.3, 0.4, 0.5 and $y = 0$, 0.2, 0.4, 0.6, 0.8, 1.0) are prepared by the chemical co-precipitation method. The chemicals used for the synthesis were $BaCl_2{\cdot}4H_2O$ (Analar 99%), $Co(CH_3COO)_2{\cdot}4H_2O$ (Merck 99%), $Fe(NO_3)_3{\cdot}9H_2O$ (Sigma–Aldrich 98%), $ZrOCl_2{\cdot}8H_2O$ (BDH 96%), $Mn(CH_3COO)_2{\cdot}4H_2O$ (Merck 98%), $Ni(CH_3COO)_2{\cdot}4H_2O$ (Merck 99%), NaOH (Merck 98%) and Na_2CO_3 (Merck 99%). Stoichiometric amounts of the constituent metal salts were mixed together in distilled water to form a homogeneous solution. The temperature of the solution was raised to 353 K under constant stirring. A mixture of NaOH and Na_2CO_3 in the ratio of 5:1 (v/v) was added drop wise to the above solution to gradually raise the pH 11 at which the precipitate was formed. The precipitate was washed thoroughly by deionized water, dried at 373 K and finally ground using an Agate mortar and pestle. The powder was finally annealed for 4 h at 1153 K with a constant heating rate of 5 K min^{-1} using a temperature programmed tube furnace. Powder X-ray diffraction analysis was carried out by a diffractometer (SmartLab by Rigaku Corp., Japan) that employs CuK_α as a radiation source. A Mössbauer (WebResearch W802, USA) drive system operating in constant acceleration mode combined with conventional electronics and ^{57}Co (Rh matrix) source of 50 mCi activity were used and the spectra were collected in transmission geometry. Morphological studies were carried out using scanning electron microscope (Hitachi S-3400N). Room temperature magnetic measurements on the samples were performed using an external field of 15 kOe. A vibrating sample magnetometer (VSM-5-15 AUTO by Toei Kogyo Co., Japan) equipped with electromagnets (TEM-WF86R-153) was employed for this purpose. For permittivity measurement, the samples of dimension of 5 mm × 1.9 mm × 0.5 mm (±0.05 mm) were placed close to the reference plane in a test fixture. The transmission line used during measurements had impedance of 50 Ω. The all shielded shorted micro-strip line method was used to measure complex permeability by network analyzer (E 8362B Agilent Technologies PNA series) with measurements' detail found elsewhere [16]. During measurements, the device under test (DUT) of dimensions 5 mm × 5 mm × 0.5 mm (±0.05), was inserted and fixed to the short end under the static applied magnetic field across the specimen. Errors due to the residual parameters of the test fixture were effectively minimized, by performing OPEN, SHORT and known LOAD calibrations on the DUT.

3. Results and discussion

3.1. X-ray diffraction and Mössbauer analysis

Fig. 1 shows powder X-ray diffraction patterns of Mn and Zr–Ni substituted W-type hexaferrite samples of nominal composition $BaCo_{2-x}Mn_xFe_{16-2y}Zr_yNi_yO_{27}$ ($x = 0.0$–0.5 and $y = 0.0$–1.0). The XRD data was used to calculate the cell constants, crystallite sizes (D_x), cell volume (V) and X-ray density (ρ_x) using equations described elsewhere [15]. The lattice/cell constants 'a' and 'c' were calculated by solving the simultaneous equations for different diffraction peaks using equation, $1/d_{hkl}^2 = 4(h^2 + hk + k^2)/3a^2 + l^2/c^2$, where h, k and l are Miller indices and d is the inter planer spacing. The values of these parameters are listed in Table 1. The bulk density (ρ_m) of the samples is measured using Archimedes principle [17] and the sample porosity is calculated as $1 - \rho_m/\rho_x$. It is observed that with the addition of the above-mentioned ions both the lattice constants and the cell volume (V) increase. This is due to relatively larger ionic radii of the dopants, i.e. Zr^{4+} (0.80 Å), Ni^{2+} (0.69 Å) and Mn^{2+} (0.80 Å), as compared to that of Fe^{3+} (0.64 Å) ions. On the other hand, the value for ρ_x remains almost constant while ρ_m slightly increases. The calculated porosity is found to decrease with the addition of the substituted ions, which is an indication of an increase in density of the samples. The materials of increased density are considered beneficial from application point of view.

Mössbauer spectra of different compositions, $BaCo_{2-x}Mn_xFe_{16-2y}Zr_yNi_yO_{27}$ ($x = 0.0$–0.5; $y = 0.0$–1.0), are shown in Fig. 2. The spectra resemble closely to the pattern for the W-type hexaferrites [1,18]. The Mössbauer spectra were

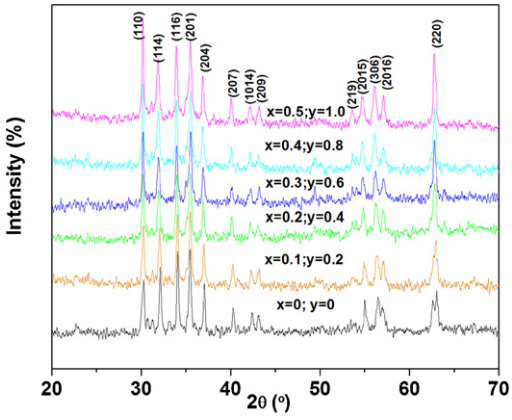

Fig. 1. X-ray diffraction patterns for $BaCo_{2-x}Mn_xFe_{16-2y}Zr_yNi_yO_{27}$ hexaferrite nanoparticles.

Table 1
Structural parameters calculated for $BaCo_{2-x}Mn_xFe_{16-2y}Zr_yNi_yO_{27}$.

Parameters	$x = 0$ $y = 0$	$x = 0.1$ $y = 0.2$	$x = 0.2$ $y = 0.4$	$x = 0.3$ $y = 0.6$	$x = 0.4$ $y = 0.8$	$x = 0.5$ $y = 1.0$
Crystallite size (D_x/nm)	45	43	38	49	46	35
Lattice constant (a/Å)	5.84	5.87	5.88	5.88	5.89	5.90
Lattice constant (c/Å)	33.33	33.34	33.37	33.49	33.68	33.91
Cell Volume (V/Å^3)	985	996	999	1004	1010	1023
X-ray density (ρ_x/g cm^{-3})	5.33	5.29	5.30	5.30	5.29	5.25
Bulk density (ρ_m/g cm^{-3})	4.69	4.71	4.93	4.91	4.95	4.99
Porosity (P/%)	12.0	10.9	6.98	7.35	6.42	4.95

fitted by superposition of Zeeman sextets for different sub-lattices by Lorentzian line analysis. The assignment of values for different sub-lattices made was according to the procedure validated for W-hexaferrites compound described in detail elsewhere [1,19]. During the fitting process, Co^{2+} ions considered distributed, were mainly on octahedral ($4f_{VI}$, 6g) sites [20,21]. Although there are seven structurally distinguishable sites in these ferrites but magnetically, only five sites were assumed for fitting because of combinations of 6g and 4f into 2b sub-lattice while those of 4e and $4f_{IV}$ into f_{IV} [19].

In case of sample with $x = 0$; $y = 0$, the 12k sub-lattice is split up in to two sub-lattices without change in the chemical shift ($k_1 = 0.224$ m ms^{-1}, $k_2 = 0.224$ m ms^{-1}) and quadrupole splitting ($k_1 = 0.191$ m ms^{-1}, $k_2 = 0.192$ m ms^{-1}). However, when dopants are added the 12k sub-lattice is unified due to change in the surroundings of Fe^{3+} ions and hence one Zeeman sextet is observed which is used for fitting. The values of the hyperfine interaction (H_{hf}) and isomer shift (δ) observed for the sample with Mn content of $x = 0.1$ and Zr–Ni content of $y = 0.2$, are 299.1 kOe and 0.732 m ms^{-1}, respectively, owing to the presence of small concentration of Fe^{2+} ions in the sample. Referring to the values of hyperfine interaction (H_{hf}) and relative area (A) for the above sample (Fig. 3a and b), the guest ions i.e. Zr^{4+}, Ni^{2+} and Mn^{2+}, are believed to have been substituted at 2d, 12k, and 2b sites with diamagnetic Zr^{4+} ions particularly substituted at 2d sites. For M-type hexaferrite, it has been reported in the literature that Zr^{4+} ions exhibit preference for bi-pyramidal sub-lattice [22]. Therefore owing to reduction in the value of H_{hf} the diamagnetic Zr^{4+} ion is

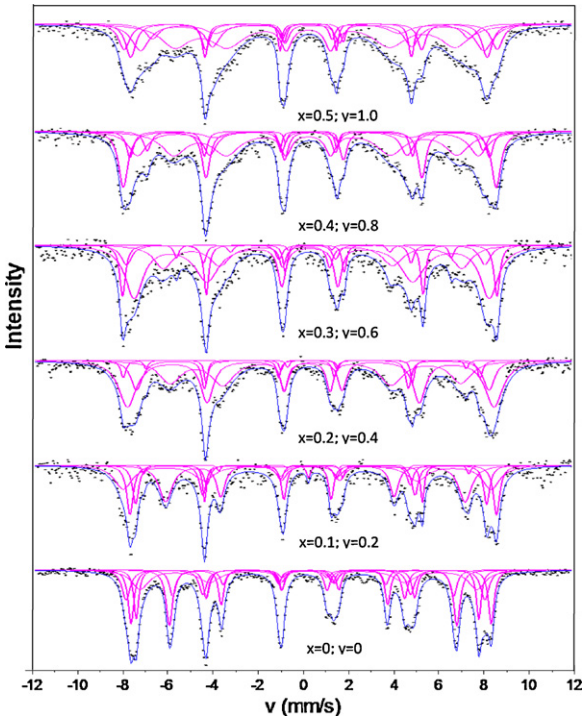

Fig. 2. Room temperature Mössbauer spectra for annealed $BaCo_{2-x}Mn_xFe_{16-2y}Zr_yNi_yO_{27}$ hexaferrites.

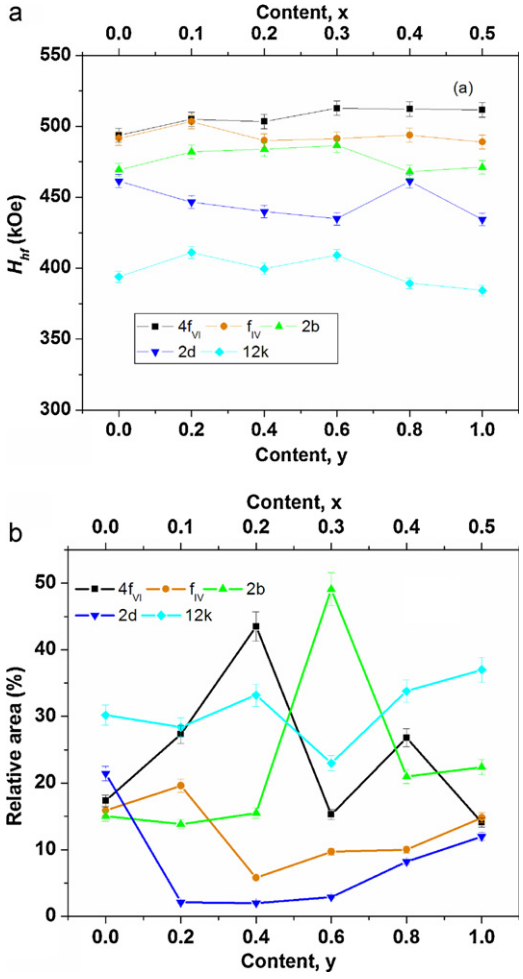

Fig. 3. (a) Variations of hyperfine interaction (H_{hf}) for different sub lattices with Mn^{2+}, Zr^{4+} and Ni^{2+} content. (b) Percentage relative area variations with Mn^{2+}, Zr^{4+} and Ni^{2+} content.

considered to occupy 2d bi-pyramidal site while Mn^{2+} and Ni^{2+} ions occupy 12k and 2b sub-lattices when the dopant contents are low. Similarly for the dopant contents of $x = 0.2$; $y = 0.4$, the substituted ions occupy f_{IV} sites and 2d site so that the hyperfine interaction values are reduced from 503.4 kOe and 446.6–490 kOe and 439 kOe, respectively. According to relative area estimated for the sample of the dopant levels of $x = 0.2$; $y = 0.4$, it can possibly be argued that Ni^{2+} and Mn^{2+} ions show preference for $4f_{VI}$ and 12k sites. However, as is evident from Fig. 3a the hyperfine interaction values are enhanced for these sub-lattices. In fact, the Co^{2+} ions have low magnetic moment compared to the incoming Mn^{2+} ions. Hence, strong antiferromagnetic interactions via superexchange path (2d)–O^{2-}–($4f_{VI}$), about 90° superexchange interactions through ($4f_{VI}$)–O^{2+}–($4f_{VI}$), and direct exchange ($4f_{VI}$)–($4f_{VI}$) due to overlap of 3d orbitals of the iron ions at $4f_{VI}$ site [23], are probably the main cause for the enhanced hyperfine interaction on these sites. This phenomenon in turn is responsible for the slight increase in the observed value of hyperfine interaction for 12k site via super-exchange path of (12k)–O^{2-}–($4f_{VI}$). Further substitution beyond $x = 0.3$; $y = 0.6$ leads to decrease in the value of hyperfine interaction for 2b and 12k sub-lattices while the value remain almost constant for $4f_{VI}$ and f_{IV} sub-lattices. The hyperfine interaction values for 2d site increase probably due to enrichment of iron ions at 2d site as could be noted from the observed percentage relative area for 2d site given in Fig. 3b.

On increase in the substituent content, average isomer shift (δ) for different sub-lattices increases and reaches a maximum value at the dopant contents of $x = 0.4$; $y = 0.8$ as shown in Fig. 4a. The phenomenon is attributed to enhancement in the value of the cell volume leading to a decrease in the charge density so that value of the isomer shift increases. Fig. 4b shows an average quadrupole splitting (ΔE) value for all the sub-lattices with minimum value for the dopant content $x = 0.2$; $y = 0.4$ as well as for $x = 0.3$; $y = 0.6$. This observation indicates that these compositions have relatively uniform and stable environment around the magnetic ions at different sub-lattices [24]. On this basis, it can be suggested that the synthesized material of the above-mentioned compositions may be suitable from technical point of view in magnetic and microwave devices.

3.2. Morphological analysis

Fig. 5a and b represents SEM images for a few selected samples of substituted $BaCo_{2-x}Mn_xFe_{16-2y}Zr_yNi_yO_{27}$ hexaferrites nanoparticles doped with Mn, Zr and Ni ionic contents

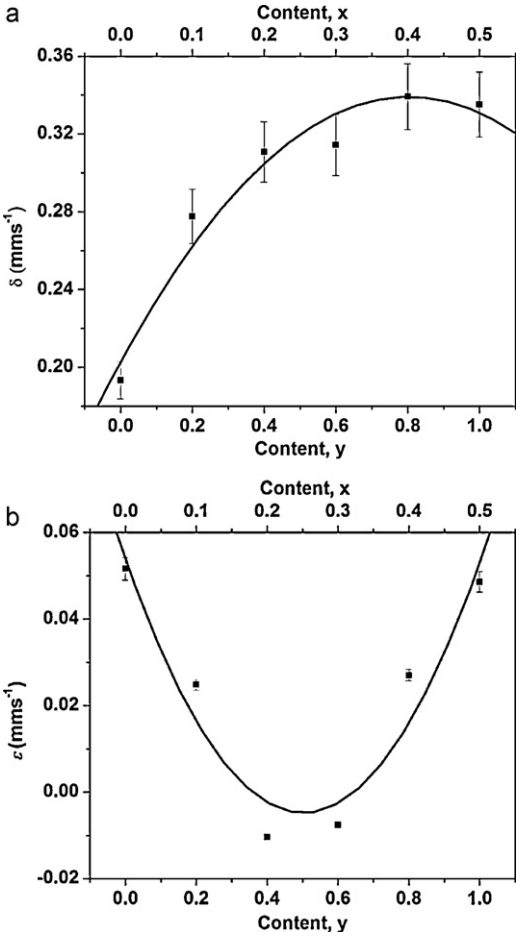

Fig. 4. (a) Average chemical shift over the sub lattices as function of content. (b) Average quadrupole splitting values over the all sites as function of content.

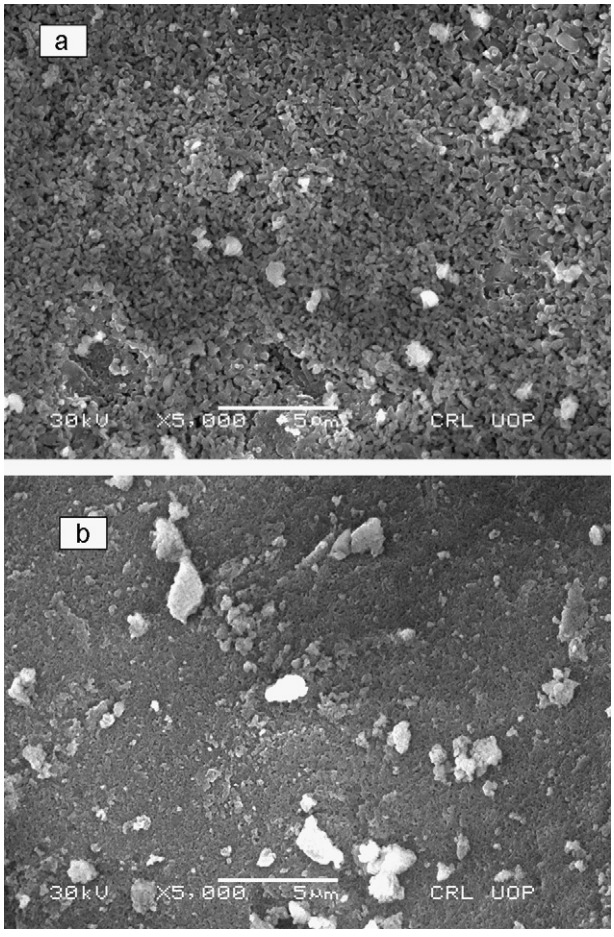

Fig. 5. Scanning electron microscopy images for (a) $BaCo_2Fe_{16}O_{27}$ and (b) $BaCo_{1.9}Mn_{0.1}Fe_{15.6}Zr_{0.2}Ni_{0.2}O_{27}$ hexaferrite samples.

of $x = 0.0,\ 0.1;\ y = 0.0,\ 0.2$. The particles in the un-doped $BaCo_2Fe_{16}O_{27}$ sample are interconnected and has a rod shape morphology with large inter granular porosity (Fig. 5a). The interconnection between the magnetic particles may be due to the interactions and alignments of the opposite magnetic poles. Fig. 5b for $BaCo_{1.9}Mn_{0.1}Fe_{15.6}Zr_{0.2}Ni_{0.2}O_{27}$ sample has more or less similar shape to that of the un-doped sample but a considerable reduction in inter-granular porosity is observed and the sample becomes densely packed. The white spots are due to the particles, which remained uncoated during the gold coating process for SEM analysis. Therefore, it can be argued that doping with Mn, Zr and Ni ions has reduced the inter-granular porosity of W-type hexaferrites while the shape of the particles remained unchanged.

3.3. Magnetic analysis

M–H loops measured at room temperature for Mn^{2+}, Zr^{4+} and Ni^{2+} substituted $BaCo_2Fe_{16}O_{27}$ hexaferrite nanoparticles are given in Fig. 6. The values of saturation magnetization (M_s), remanent magnetization (M_r) and coercivity (H_c) for the synthesized compositions are plotted versus the dopant contents of x and y (Fig. 7). The values of M_s and M_r for the undoped sample, i.e. $BaCo_2Fe_{16}O_{27}$ ($x = 0$, $y = 0$) are 61.9 emu g^{-1} and 31.9 emu g^{-1}, respectively, but they increase to values of 79.8 emu g^{-1} and 36.0 emu g^{-1}, respectively, when the dopant contents are $x = 0.3$; $y = 0.6$. Further addition of the dopants up to $x = 0.5$; $y = 1.0$ reduces these values to 56.0 emu g^{-1} (M_s) and 23.7 emu g^{-1} (M_r). The H_c values continuously decrease from the value of 1.87 kOe for un-doped sample to 0.805 kOe up to the dopant contents of $x = 0.5$; $y = 1.0$.

As mentioned in Section 3.1, Zr^{4+} ions exhibit preference for 2d bi-pyramidal site (spin up) and f_{IV} tetrahedral sub-lattices (spin down) while Mn^{2+} and Ni^{2+} ions occupy octahedral $4f_{VI}$ (spin down) sites, 12k (spin up) and 2b (spin up) sub-lattices. The initial increase in M_s from a value of 61.9 emu g^{-1} to 79.8 emu g^{-1} is due to increase in the resultant spin along the *c*-axis. Although cations at bi-pyramidal 2d site have upward spin but f_{IV} which is a combination of 4e and $4f_{IV}$ have cationic spin downward along the *c*-axis. Therefore diamagnetic Zr^{4+} ions

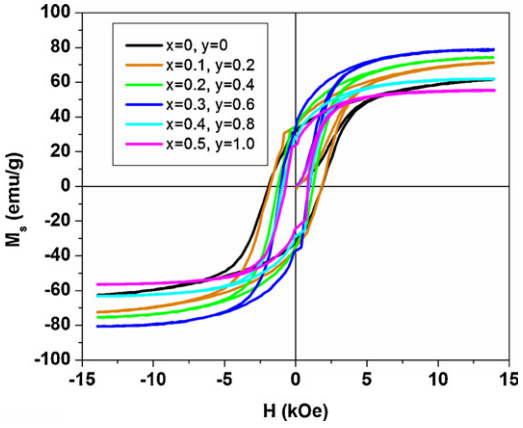

Fig. 6. *M–H* loops measured at room temperature for $BaCo_{2-x}Mn_xFe_{16-2y}Zr_yNi_yO_{27}$.

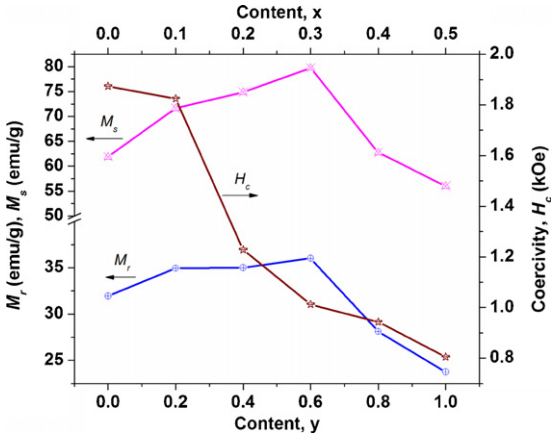

Fig. 7. Composition dependence of Saturation magnetization (M_s), remanent magnetization (M_r) and coercivity (H_c) for synthesized samples.

with magnetic moment $\mu_B = 0$, result in diminishing of downward spin at 4e and $4f_{IV}$ that increases the saturation magnetization. Theoretically, the above-mentioned preference of Mn^{2+} ($4f_{VI}$, 2b) and Ni^{2+} (12k and 2b) ions for different sub-lattices suggests a negative contribution to the overall value of the saturation magnetization. However, continuous increase in M_s value can be attributed to the enhancement of the hyperfine exchange interactions for different sub-lattices as discussed in Section 3.1 (Fig. 3a). Although beyond the dopant content level of $x = 0.3$; $y = 0.6$, the value for hyperfine interaction for 2d site increases while those for $4f_{VI}$ and f_{IV} remain constant. The possible cause for further decrease in the measured value for M_s is believed to be the reduction of the resultant spin along the easy axis *c*-direction. The maximum value obtained for remanent magnetization, M_r is 36.0 emu g^{-1} while a minimum value of 23.7 emu g^{-1} is obtained for a composition with $x = 0.5$; $y = 1.0$. Most of the time compromise is to be made between the value for remanent magnetization and coercivity of material. It is because the enhancement of M_r involves the annealing of material at higher temperatures, which results in decrease in the coercivity due to grain growth associated with high annealing temperatures. Hence, a composition $BaCo_{1.7}Mn_{0.3}Fe_{14.8}Zr_{0.6}Ni_{0.6}O_{27}$ with $M_s = 78.9$ emu g^{-1}, $M_r = 36.0$ emu g^{-1} and $H_c = 1.01$ kOe can be considered promising for use as high density magnetic data storage media. The reason that coercivity (H_c) regularly decreases is the expected lowering of magneto crystalline anisotropy due to substitution of non-magnetic Zr^{4+} ions. Because coercivity of material is directly related to the magneto crystalline anisotropy (H_a) and for uniaxial hexagonal compounds with $k_1 \gg k_2$, H_a is given by an equation [25]; $H_a = 2k_1/M_s$, where k_1 is the first anisotropy constant and M_s is the saturation magnetization. In this equation anisotropy constant is dependent on M_s values as well which may be one of the reasons for the observed sharp decrease in the value of coercivity with increase in the dopant concentration (Fig. 7).

3.4. Microwave absorption characteristics

Complex relative permittivity $\varepsilon_r = \varepsilon' - j\varepsilon''$ and permeability $(\mu_r = \mu' - j\mu'')$ are the two parameters that are usually

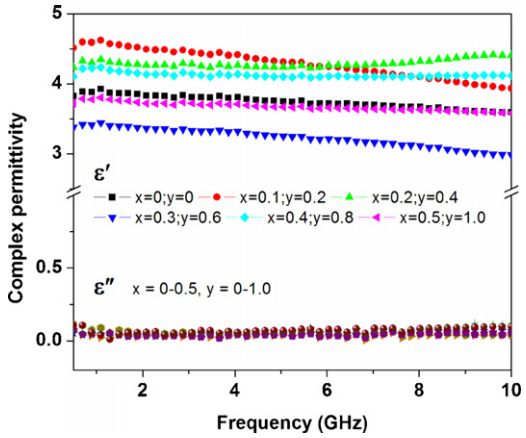

Fig. 8. Complex relative permittivity spectra ($\varepsilon_r = \varepsilon' - j\varepsilon''$) having real and imaginary part as function of frequency.

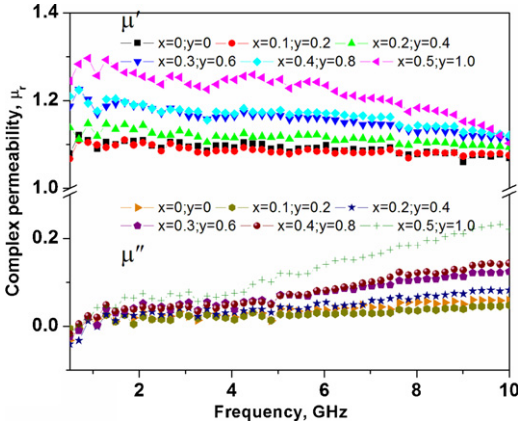

Fig. 9. Complex relative permeability spectra ($\mu_r = \mu' - j\mu''$) having real and imaginary parts as function of frequency.

varied to design an absorber for attenuation of electromagnetic radiations at microwave frequencies. Complex relative permittivity for $BaCo_{2-x}Mn_xFe_{16-2y}Zr_yNi_yO_{27}$ (where $x = 0.0$–0.5 and $y = 0.0$–1.0), in a range of 0.5–10 GHz are shown in Fig. 8. The figure shows that the imaginary part of permittivity (ε'') remains very low throughout the measurement range for all the investigated samples. The average value for the real part of permittivity (ε') in the synthesized samples shows slight variation with the addition of the dopants. The average value of ε' is the highest for the sample of dopant content x; $y = 0.1$; 0.2, while the sample of content $x = 0.3$, $y = 0.6$ exhibits the lowest average ε' value. Moreover, the real part of complex permittivity remains almost constant for $x = 0.2$; $y = 0.4$ and $x = 0.4$; $y = 0.8$, while that for the other samples show regular decrease with increase in frequency. At low frequency, both dipolar and interfacial polarization contribute to the value of ε' but at higher frequency, only the electronic polarization (intrinsic polarization) becomes significant. When the intensity of frequency is low the electron exchange between the ions Fe^{2+} and Fe^{3+} follow the alternating field but if the intensity of the applied frequency is further increased the hoping of electrons between two ions cannot follow the alternating field and the conduction lag behind. Therefore, the value for the real part of complex permittivity is higher at low frequencies and its value become lower at high frequencies [6]. Mössbauer analysis described in Section 3.1 indicates that the W-type hexaferrite sample composition of $x = 0.1$; $y = 0.2$ have some Fe^{2+} ions at octahedral sites and probably are responsible for high value of ε'. In ferrites, it usually found is that the presence of Fe^{2+} ions stands responsible for increase in ε' value because the ferrous ions are comparatively more polarizable to that of ferric ions. The formation of Fe^{2+} ions at content $x = 0.1$; $y = 0.2$, is due to the transfer of electrons between Ni^{2+} and Fe^{3+} to form a pair of Ni^{3+} and Fe^{2+} which produces the conditions for high permittivity. At this composition the concentration of Mn^{2+} ions are very low to convert the Fe^{2+} ions again to Fe^{3+} ions. However at high concentration of level $x = 0.3$; $y = 0.6$ the average low value of permittivity is due to the energetically favorable electronic transition at octahedral site through following mechanism [3].

$$Ni^{3+} + Mn^{2+} \rightarrow Ni^{2+} + Mn^{3+}$$

$$Fe^{2+} + Mn^{3+} \rightarrow Fe^{3+} + Mn^{2+}$$

The complex relative permeability spectra for all synthesized sample are plotted as function of frequency in Fig. 9. Both real (μ') and imaginary (μ'') parts of permeability increase constantly with the addition of Mn^{2+}, Zr^{4+}, and Ni^{2+} ions in the main skeleton of $BaCo_2Fe_{16}O_{27}$ hexaferrite. The imaginary part of permeability (μ'') is directly proportional to the saturation magnetization (M_s) and inversely proportional to the anisotropy field (H_a) value by an equation [6]; $\mu'' = M_s/(2H_a\alpha)$, where α is the extinction coefficient. With the increased substitution, the M_s value increased while diamagnetic Zr^{4+} ions are responsible for reduction in the anisotropy constant value which is probably the cause of increased magnetic loss. The high value for real part of complex permeability (μ') is also perhaps due to the increase in the saturation magnetization up to $x = 0.3$; $y = 0.6$, which is because of increasing resultant magnetic moment along the c-axis. Further enhancement in the value of μ' is due to increase in the hyperfine interaction on various sites as can be observed in Fig. 3a.

Fig. 10 shows reflection loss (dB) for different compositions of synthesized W-type hexaferrites at optimal thicknesses. The matching thickness, in millimeters, used for different absorber compositions from x; $y = 0.0$ through x; $y = 0.5$; 1.0, in millimeters, are 4.9, 4.6, 4.3, 4.9, 4.5 and 4.4. The equations used for calculating the reflection loss could be found elsewhere [26]. For absorber to attenuate electromagnetic radiations is generally designed as to maximize the real part of permeability while real part of permittivity should be minimized so that these parameter become close to each other for attaining the matching conditions [7]. From Fig. 10 it is found that minimum reflection loss of 14.85 dB at an optimum matching thickness of 4.4 mm, is obtained in case of highly doped sample with composition $x = 0.5$; $y = 1.0$. The high absorption of this sample is due to comparatively large real and imaginary part of permeability.

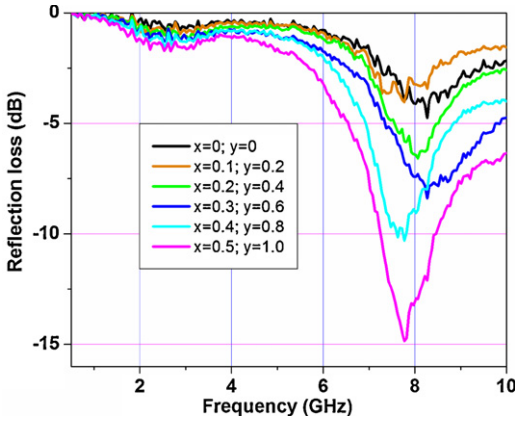

Fig. 10. Microwave absorption spectra for $BaCo_{2-x}Mn_xFe_{16-2y}Zr_yNi_yO_{27}$ hexaferrite nanoparticles.

4. Conclusions

Pure $BaCo_2Fe_{16}O_{27}$ hexaferrites doped with Mn^{2+} ions on divalent Co^{2+} ionic sites and combinations of Zr^{4+} and Ni^{2+} ions on trivalent iron sites, are synthesized by chemical co-precipitation technique. Mössbauer analysis indicated that Zr^{4+} ions occupy 2d site at lower concentration and f_{IV} ions at higher doped content. Mn^{2+} and Ni^{2+} ions prefer 12k, 2b and $4f_{VI}$ sub-lattices. Considerable enhancements were achieved both in values for M_s and M_r due to dopant ions, allowing the usage of these materials as potential candidate for data storage and perpendicular recording media. More than 90% absorption is obtained so that these materials are equally suitable for self-attenuating electromagnetic radiations for high frequency devices.

Acknowledgment

The project is supported by Higher Education Commission (HEC) of Pakistan.

References

[1] G. Albanese, M. Carbucicchio, G. Asti, Spin-order and magnetic properties of $BaZn_2Fe_{16}O_{27}$ (Zn_2-W) hexagonal ferrites, Appl. Phys. 11 (1976) 81–88.
[2] A.P. Lilot, A. Gerard, F. Grandjean, Analysis of the superexchange interactions paths in the W-hexagonal ferrites, IEEE Trans. Magn. Magn. 18 (1982) 1463–1465.
[3] J. Smit, H.P.J. Wijin, Ferrites Physical Properties of Ferromagnetic Oxides in Relation to Their Technical Applications, Wiley, Netherlands, 1959.
[4] M.A. Ahmad, N. Okasha, R.M. Kershi, Dramatic effect of rare earth ion on the electrical and magnetic properties of W-type barium hexaferrites, Physica B 405 (2010) 3232–3233.
[5] J. Xu, H. Zou, H. Li, G. Li, S. Gan, G. Hong, Influence of Nd^{3+} substitution on the microstructure and electromagnetic properties of barium W-type hexaferrite, J. Alloys Compd. 490 (2010) 552–556.
[6] X. Huang, J. Chen, J. Zhang, L. Wang, Q. Zhang, A new microwave absorber based on antimony-doped tin oxide and ferrite composite with excellent electromagnetic match, J. Alloys Compd. 506 (2010) 347–350.
[7] Y.P. Wu, C.K. Ong, G.Q. Lin, Z.W. Li, Improved microwave magnetic and attenuation properties due to the dopant V_2O_5 in W-type barium ferrites, J. Phys. D: Appl. Phys. 39 (2006) 2915–2919.
[8] D.M. Hemeda, A. Al-Sharif, O.M. Hemeda, Effect of Co substitution on the structural and magnetic properties of Zn-W hexaferrite, J. Magn. Magn. Mater. 315 (2007) L1–L7.
[9] M.A. Ahmad, N. Okasha, M. Oaf, R.M. Kershi, The role of Mg substitution on the microstructure and magnetic properties of BaCoZnW-type hexagonal ferrites, J. Magn. Magn. Mater. 314 (2007) 128–134.
[10] H. Zhang, Z. Liu, X. Yao, L. Zhang, M. Wu, The synthesis, characterization and microwave properties of ZnCo-substituted W-type barium hexaferrite, from a sol–gel precursors, J. Sol–Gel Sci. Technol. 27 (2003) 277–285.
[11] R.B. Jotania, R.B. Khumane, C.C. Chauhan, S.K. Menon, B.D. Kulkarni, Synthesis and magnetic properties of barium–calcium hexaferrite particles prepared by sol–gel and microemulsion techniques, J. Magn. Magn. Mater. 320 (2008) 1095–1101.
[12] E.P. Naiden, R.A. Zhuravlyov, V.I. Itin, O.G. Terekhova, M.V. Politov, Y.M. Lopushniak, V.E. Tcherbakov, Magnetic properties of hexaferrite nanosized powders produced via mechanoactivation, Sci. Sinter. 37 (2005) 107–114.
[13] D. Lisjak, A. Znidarsic, A. Sztanislav, M. Drofenik, A two-step synthesis of NiZn-W hexaferrites, J. Eur. Ceram. Soc. 28 (2008) 2057–2062.
[14] W. Jing, Z. Hong, B. Shuxin, C. Ke, Z. Changrui, Microwave absorbing properties of rare-earth elements substituted W-type barium ferrite, J. Magn. Magn. Mater. 312 (2007) 310–313.
[15] M.J. Iqbal, R.A. Khan, Enhancement of electrical and dielectric properties of Cr doped $BaZn_2$ W-type hexaferrite for potential application in high frequency devices, J. Alloys Compd. 478 (2009) 847–852.
[16] S. Takeda, H. Suzuki, Wideband measurement system of ΔH_ω using all shielded shorted microstrip line, J. Magn. Soc. Jpn. 33 (2009) 171–174.
[17] M.M. Barakat, M.A. Henaish, S.A. Olofa, A. Tawfiq, Sintering behavior of the spinel ferrite system $Ni_{0.65}Zn_{0.35}Fe_{2-x}Cu_xO_4$, J. Therm. Anal. 37 (1991) 241–248.
[18] A. Paoluzi, F. Licci, O. Moze, G. turilli, A. Deriu, G. Albanese, E. Calabrese, Magnetic, Mossbauer, and neutron diffraction investigation of W-type hexaferrite $BaZn_{2-x}Co_xFe_{16}O_{27}$ single crystal, J. Appl. Phys. 63 (1988) 5074–5080.
[19] L.D. Xin, Z.N. Nin, G.S. Jiao, L.G. Dong, W.H. Zong, Magnetic and Mossbauer study of (TiCu)Ni_2W hexagonal ferrite system, IEEE Trans. Magn. 25 (1989) 3290–3292.
[20] J.M.L. Breton, J. Teillet, G. Wiesinger, A. Morel, F. Kools, P. Tenaud, Mossbauer investigation of Sr–Fe–O hexaferrites with La–Co addition, IEEE Trans. Magn. 38 (2002) 2952–2954.
[21] A. Collomb, P. Wolfers, X. Obradors, Neutron diffraction studies of some hexagonal ferrites: $BaFe_{12}O_{19}$, $BaMg_2$-W and $BaCo_2$-W, J. Magn. Magn. Mater. 62 (1986) 57–67.
[22] M.V. Rane, D. Bahadur, A.K. Nigam, C.M. Srivastava, Mossbauer and FT-IR studies on non-stoichiometric barium hexaferrites, J. Magn. Magn. Mater. 192 (1999) 288–296.
[23] C. Sauer, U. Kobler, W. Zinn, H. Stablen, High field Mossbauer effect study of $LaFe_{12}O_{19}$, J. Phys. Chem. Solids 39 (1978) 1197–1201.
[24] S.Y. An, I.B. Shim, C.S. Kim, Mossbauer and magnetic properties of Co–Ti substituted barium hexaferrite nanoparticles, J. Appl. Phys. 91 (2002) 8465–8468.
[25] Z.W. Li, C.K. Ong, Z. Yang, F.L. Wei, X.Z. Zhou, J.H. Zhao, A.H. Morrish, Site preference and magnetic properties for a perpendicular recording material: $BaFe_{12-x}Zn_{x/2}Zr_{x/2}O_{19}$ nanoparticles, Phys. Rev. B 62 (2000) 6530–6537.
[26] M.J. Iqbal, R.A. Khan, S. Takeda, S. Mizukami, T. Miyazaki, W-type hexaferrite nanoparticles: a consideration for microwave attenuation at wide frequency band of 0.5–10 GHz, J. Alloys Compd. 509 (2011) 7618–7624.